The `lion-msc` document class

THESIS

submitted in partial fulfillment of the
requirements for the degree of

BACHELOR OF SCIENCE
in
PHYSICS

Author : Sebastiaan Van Mulken
Student ID : use \studentid{...} to define
Supervisor : use \supervisor{...} to define
2nd corrector : use \corrector{...} to define

Leiden, The Netherlands, April 6, 2017

The `lion-msc` document class

Sebastiaan Van Mulken

Huygens-Kamerlingh Onnes Laboratory, Leiden University
P.O. Box 9500, 2300 RA Leiden, The Netherlands

April 6, 2017

Abstract

Please use \abstract{...} to define an abstract in the document preamble.

Contents

Description of the document class lion-msc

This chapter describes the lion-msc document class. The aim of this document class is to assist staff, students and the university administration with the creation of bachelor and master theses. By using this document class we create a document that has a first page that contains all required information such as title, author, student ID, supervisor, second corrector etc.

Some of the compulsory features are standardized, many other have default values. More experienced LaTeXusers can easily modify the feel and look of the document, but should try not too modify the first pages of the thesis. This is the page that should be handed in to the university administration that keeps this on file together with the grade given by the staff member of the physics department.

At a later stage all bachelor and master theses will be placed in an online repository that is, in principle, publicly available. This repository will look better (more professional) if the first pages and layout of theses is similar.

The use of a specialized document class is a method that is used by many scientific journals to ensure that all submitted articles contain all necessary information. Publishers only accept articles that are typeset according to certain rules. LaTeXstyle files and templates are often provided to help authors to comply with the style of the journal.

Currently the document class is still under active development and will be improved. If you use this style to typeset your thesis please do check frequently for updates of the files lion-msc.cls and the associated bibliography style file lion-msc.bst.

1

1.1 Getting Started

Unzip the zip file into a directory and start with the file minimal.tex. On most systems this should compile if you have the 'lion-msc.cls' file and 'minimal.tex' in the same working directory. 'lion-msc' is based on the report class and any valid option for a report can be passed onto lion-msc. In addition, lion-msc uses several additional packages. Most modern LaTeXsystems have features that allow you to automatically get missing files if your computer is connected to the internet.

A minimal LaTeXdocument that should compile with pdfLaTeXis the following (I called this file 'minimal.tex')

```
\documentclass[twoside,single]{lion-msc}

\title{Title}
\author{A. Uthor}

\begin{document}

\maketitle

\chapter{Chapter 1}

Here you type the text for the first chapter of
your thesis.

\end{document}
```

If problems arise at this point check if you compile LaTeXdirectly to pdf. The older route that converts tex files to dvi files and then to postscript is not supported. It is very unlikely that this will be supported in the future.

If problems persist check if you have all necessary files in the right location, most notably 'lion-msc.cls' and 'logo-leidenuniv.pdf'. If you placed the files in some standard location for your tex installation make sure that your installation knows about these files. A quicker, more fail-safe way around this is to place these files in the same working directory as the LaTeXfile that you are trying to compile.

Once you have made these steps take a look at lion-msc.tex as it contains a more complete template that shows how to use the lion-msc documentclass.

1.1.1 Files in this package

The files included with this package are the following:

lion-msc.cls	documentclass file
logo-leidenuniv.pdf	PDF file with logo of Leiden University. This file is required by the document class
lion-msc.bst	bibliography style file that can be used with bibtex
minimal.tex	Minimal LaTeXfile demonstrating the use of lion-msc.cls
AlexanderPRA.tex	LaTeXfile used as an example of a Master Thesis
lion-msc.tex	This file
lion-msc.pdf	PDF file of the compiled version of lion-msc.tex
thesisstyle.jpg	Image used for the cover
Fig1.png	Figure used in AlexanderPRA.tex
Fig2.png	Figure used in AlexanderPRA.tex
Fig3a.png	Figure used in AlexanderPRA.tex
Fig3b.png	Figure used in AlexanderPRA.tex
Fig4.png	Figure used in AlexanderPRA.tex
4photon.bib	BibTeX database file for AlexanderPRA.tex

1.2 List of available commands and options

This section gives an overview of special commands and options that are defined through this documentclass. You can use these to change the appearance of your thesis and to include all necessary information.

1.2.1 lion-msc options

Lion-msc inherits and passes its options to the report class. By default the class uses [a4paper, 12pt, fleqn]. If desired this can be passed on by including valid report class options to the options of lion-msc.

double	(default) double line spacing, useful for drafts
single	single line spacing. This looks better in the final version

1.2.2 lion-msc commands

With the lion-msc documentclass most of the required information is entered in the preamble of the LaTeXdocument (i.e. before \begin{document}). This information is made visible by using the \maketitle command. This should be the first command after \begin{document}.

Note that you have to fill out the required options. If you leave these empty, instructions will appear in red on the title page. Most of these commands are quite flexible. For instance you can insert newline characters (\\) in the affiliation command. This is practical if you do a project outside LION.

\author	(required) Defines the author
\title	(required) Defines the title of your thesis
\abstract	(required) Provide your abstract here, making sure that it fits on the page.
\affiliation	Sets the affiliation to something else than the default value.
\address	Use this to change the default address if needed.
\studentid	(required) enter your student ID (studentnummer)
\supervisor	(required) provide a valid supervisor. This should be a staff member of the Leiden Physics Department
\corrector	(required) provide the name of the 2nd corrector. This could be an external supervisor.
\degree	(optional) Default is "Bachelor of Science" Use this to change the default value.
\major	(optional) Default is "Physics" Use this to change the default value.
\coverpicture	(optional) Insert a cover picture on the first page Usage: \coverpicture{\includegraphics[width=13cm]{picture.jpg}}

Note that these commands are highly flexible and a bit a LaTeXknowledge will allow you to make all kinds of smart modifications. A common, and reasonable desire is to give credit to the PhD student or postdoc that guided you during the project. You can do this by trying the following code:

\supervisor{PhD student \\ \hspace*{\fill}Supervisor}.

Note that you should always have a staff member from Leiden as your supervisor because this person is authorized to give you the final grade.

1.2.3 Packages and additional styling tips

This documentclass uses a number of standard packages, such as amsmath, amssymb for extra functions and symbols to display math and the graphicx package to display graphics in the document. It uses the natbib package to deal with references to automatically sort and compress multiple references. I do not recommend making changes to this in the document preamble. In particular the interplay between natbib and the

bibliography style can give very unexpected results.

The default configuration also uses the hyperref package to create a pdf with hyperlinks. The links are hidden so that the text looks normal; try clicking one of the references or in the table of contents and you will see that you are automatically brought to the appropriate reference or section.

The use of packages inside the documentclass can cause an error when you try to use a package within your LATEXdocument. This typically happens when both the documentclass and your own LATEXdocument use some options. There is a \PassOptionsToPackage command that you can use before the \documentclass to try to pass the desired option to the package.

Headers with fancyhdr

The headers and footers on each page contain some useful info. This is done using the `fancyhdr` package. You can change the appearance of these by using the \fancyhead and \fancyfoot commands. See the `fancyhdr` documentation for details. You can also open lion-msc.cls in a text editor and look for these commands. You can place your own commands before the \begin{document} command in your LATEXfile. The grey text at the bottom with date and time is there to help you and your supervisor to keep track of the version, so that we do not end up correcting an old version. It may look somewhat strange in the final version and can be removed by using
\fancyfoot[CE,CO]{}.

Table of contents styling

Some people may want to get the original dots back into the table of contents. There is an old-fashioned way of doing this without extra packages. Insert the following in the document preamble. The separation of 4.5 is the default value and can be changed to tune the spacing between dots.

```
\makeatletter
\renewcommand\@dotsep{4.5}
\makeatother
```

An alternative is to use the `tocloft` package that offers additional styling options. Insert the following to use this package. (Suggestion by Casper Remeijer)

```
\usepackage{tocloft}
\renewcommand{\cftchapdotsep}{\cftdotsep}
```

Subfigures

It can be quite useful to have multiple figures next to each other. This can be done with the subcaption package. (Suggestion by Casper Remeijer)

```
\usepackage[labelformat=simple,justification=centering]{subcaption}
\renewcommand\thesubfigure{(\alph{subfigure})}
```

Spatially entangled 4-photons states from a periodically poled KTP crystal

The contents of this chapter serve as an example and are based on a scientific paper published as Phys. Rev. A **85**, 043837 (2012). This article contains results from the master thesis of Alexander J.H. van der Torren. The results and data analysis of the original master theses have been reproduced, extended and improved by S. Cigdem Yorulmaz at a later stage.

Photon pairs produced via spontaneous parametric down-conversion (SPDC) in a non-linear crystal give rise to strong nonclassical correlations. The resulting entangled photons are an important resource in quantum information, fundamental tests of quantum mechanics and have been used in experiments that demonstrate the violation of Bell's inequality, quantum teleportation and quantum communication. While most experiments focus on discrete polarization entanglement, quantum states of two particles that are entangled in continuous variables [1] such as frequency [2, 3], time-bin [4–6] or photon momenta [7–10] are also possible, which gives access to high-dimensional entanglement that can be explored by measuring correlations between two photons.

In this article, we focus on spatial entanglement using photon momenta as a continuous variable. Unlike other forms of continuous vari-

able entanglement, the quantum correlations in spatial entanglement can be resolved with relative ease and high resolution by using a combination of lenses and apertures only. The low conversion efficiency in non-linear crystals combined with the long coherence time of a continuous wave pump and ultrashort coherence time of the photon pairs ensure that most experiments are well described by two-photon interference of individual pairs [10]. As a consequence, spatial entanglement with more than two photons has remained elusive and spatial correlations beyond independent photon pairs have not been addressed in an experiment [11]. These multi-photon states are of interest since they provide access to non-trivial entanglement between more than two particles [12, 13]. Furthermore, the generation rate of four photon states sets fundamental limits on the visibility achievable in two-photon interference experiments [14] and the maximum attainable key generation rate in quantum key distribution protocols.

Here we investigate events where four spatially entangled photons are generated by SPDC. These four photons can either be two independent pairs, or they may all be in the same set of spatial and temporal modes to create a true four-photon state [5, 6]. The production of these four photon states is enhanced by the physical process of stimulated emission of a second photon pair into the same optical mode as the first pair. In the ideal situation of a single temporal and spatial mode, stimulated emission enhances the pair production rate by a factor of two compared to the probability to generate four photons in the same mode via two independent spontaneous processes. For a multi-mode situation, the relative importance of the stimulated emission process is given by a "visibility" χ that ranges from 0 to 1.

The distinction between two independent pairs and four-photon states has been addressed in the time-domain using time-bin entanglement with a pulsed laser source [5, 6]. These experiments are restricted to a single spatial mode and therefore do not allow use of spatial degrees of freedom to explore the process of stimulated emission. The total number of modes is then given by the available temporal modes and is directly related to the frequency bandwidth of the SPDC light as compared to the frequency bandwidth of the pulsed laser source [6]. To directly resolve the underlying mode structure requires a measurement of quantum correlations within a single laser pulse. Such a direct measurement of the arrival time would require detectors with high quantum efficiency and sub-picosecond timing resolution, which is well outside reach of current single-photon detector technology [15, 16]. Instead, we use spatially entangled multi-photon states that allow us to resolve the fine structure of

stimulated pairs emitted in a single laser pulse in a straightforward way. Using pinholes the momentum resolution in the far-field of the SPDC source may be made arbitrarily high. In an experiment, there is always a trade-off between the size of the pinhole and the collected signal, which sets the time required to measure coincidence rates to a sufficient level of accuracy.

2.1 Stimulated emission of spatially entangled 4-photon states

The downconversion process in the PPKTP crystal that generates photon pairs in N spatial modes can be described by an interaction Hamiltonian of the SPDC process given by [17, 18]:

$$H = \kappa \sum_i^N a_{\mathbf{q_i}}^\dagger a_{-\mathbf{q_i}}^\dagger + \text{h.c.}, \tag{2.1}$$

where $a_{\mathbf{q_i}}^\dagger$ is the creation operator that creates a single photon in a spatial mode labeled by the transverse wavevector $\mathbf{q_i}$. The operator $a_{\mathbf{q_i}}^\dagger a_{-\mathbf{q_i}}^\dagger$ thus creates a pair of photons that is correlated in their transverse photon momenta and forms the basis for spatial entanglement. The parameter κ describes the strength of the non-linear interactions and contains, among others, the (time-dependent) field of the pump and the effective non-linearity of the PPKTP crystal. For our purpose, where we pump the crystal with an intense pulsed laser, κ can be assumed to be a classical quantity. The corresponding wavefunction of the state generated by SPDC can be directly obtained from the Hamiltonian:

$$|\Psi\rangle = \exp(-iH\frac{t}{\hbar})|0\rangle \approx (1 - \frac{it}{\hbar}H - \frac{t^2}{2\hbar^2}H^2)|0\rangle,$$

where we limited the Taylor expansion in the last step to exclude quantum states with more than 4 photons. The linear term in the Taylor expansion creates a state $|\Psi_2\rangle$ that consists of a superposition of a single photon pair in any of the available spatial modes:

$$|\Psi_2\rangle = \frac{-it}{\hbar}H|0\rangle = \frac{-i\kappa t}{\hbar} \sum_{i=1}^N |1_{\mathbf{q_i}}; 1_{-\mathbf{q_i}}\rangle.$$

Please note that we use a shorthand notation in which we leave out all spatial modes without a photon. The spatial modes that contain photons

are numbered by the number of photons in that mode and the subscript refers to the transverse photon momentum of that mode. The quadratic term gives rise to a state $|\Psi_4\rangle$ with 4 photons that contains all double pair contributions, which can be represented using the same notation [6] as

$$
\begin{aligned}
|\Psi_4\rangle &= \frac{-\kappa^2 t^2}{2\hbar^2}\Bigg(2\sum_{i=1}^{N}|2_{\mathbf{q_i}};2_{-\mathbf{q_i}}\rangle + \\
&\qquad \sum_{i=1}^{N}\sum_{j=1,i\neq j}^{N}|1_{\mathbf{q_i}},1_{\mathbf{q_j}};1_{-\mathbf{q_i}},1_{-\mathbf{q_j}}\rangle\Bigg).
\end{aligned}
$$

The effect of stimulated emission follows directly from the creation operators and is contained in the extra factor $\sqrt{2}$ when two photon pairs are created in the same spatial mode.

A measurement of a single photon in a particular spatial mode with wavevector $\mathbf{q_i}$ determines the wavevector of the twin photon and corresponds to a state projection: $a_{\mathbf{q_i}}|\Psi\rangle$. The state projection allows us to calculate the probabilities of creating a single photon pair P_2 as well as the probability P_4 to create a state with 4 photons in the same mode. For a single spatial and temporal mode, the probability P_4 is exactly equal to P_2^2 and is thus enhanced by a factor 2 compared to stimulated emission of two photon pairs in the same spatial modes. In a situation with more than one spatial mode, which is of interest here, stimulated emission enhances the probability P_4 by a factor $(1+\chi)$, where χ is a "visibility" from 0 to 1 that quantifies the extra contribution to the 4 photon states due to stimulated emission. The probability to create a 4 photon state with the photons in the same mode can then be expressed as [6]:

$$
P_4 = \frac{P_2^2}{2}(1+\chi). \tag{2.2}
$$

2.2 Experimental investigation of 4-photon quantum correlations

2.2.1 Experiment

Figure 2.1 depicts the setup to explore the spatial quantum correlations due to stimulated emission of pairs in a four-photon state. In order to get a non-negligible rate of double pairs we use a highly efficient, 2 mm long, periodically poled KTP (PPKTP) crystal [19] pumped by $\sim$100 mW of 413.2 nm pulsed laser light. The pulsed laser in our setup produces 2
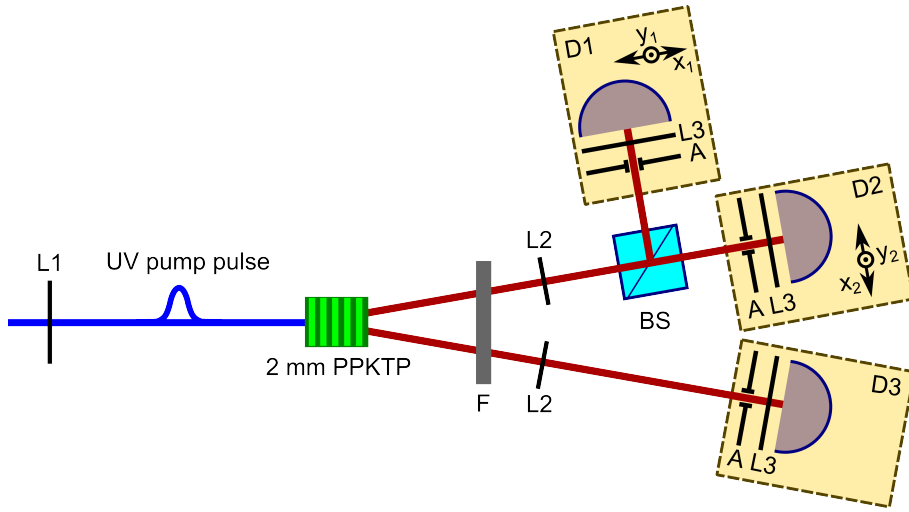
Figure 2.1: *(Color online) Setup to measure spatially entangled 4-photon states via parametric downconversion in a 2 mm PPKTP crystal. UV pump pulses from a frequency doubled Ti:Sapphire laser are focused by lens L1 (f_1 = 250 mm). Photons are collected by the lenses L2 (f_2 = 270 mm) and detected by the detector assemblies D1 − D3 that use photon counting APDs to detect single photons in a particular direction defined by the apertures A placed in the combined focal planes of L2 and L3 (f_3 = 4.5 mm). The beamsplitter, BS, allows to record if two photons are in the same spatial mode. To this end detector assemblies D1 and D2 are placed on computer controlled translation stages. Correlations in the coincidence events are due to 4-photon states that are created by the process of stimulated emission of photon pairs.*

ps pulses and is focussed into the PPKTP crystal using a lens $L1$, with a focal length f of 250 mm. The source creates non-colinear, frequency degenerate photon pairs at a wavelength of 826.4 nm that are filtered by a bandpass filter F and collected by lenses $L2$ (f = 270 mm). Three detector assemblies $D1 - D3$ are used to collect single photons with a well-defined momentum. Each of these assemblies consists of a lens $L3$ (f_3 = 4.5 mm), an aperture A placed in the far-field to select the photon momentum and a (multi-mode) fiber-coupled single photon counting avalanche photodiode (Perkin-Elmer SPCM-AQ4C). The mode diameter of the fiber used in the experiments is 50 μm and lenses $L2$ and $L3$ provide a $60\times$ magnification factor. Coincidence detection with a $\sim$1.7 ns coincidence window between the detectors $D1$ and $D3$ (or $D2$ and $D3$) results in a measurement of spatial entanglement of single pairs. The beamsplitter, BS, allows us to record coincidence events between detectors $D1$ and $D2$ that are due to two photons from different pairs. To record the spatial correlations both detector assemblies $D1$ and $D2$ are placed on computer controlled translation stages that allow movement in the x and y directions transverse to the optical beam.

The essential feature of the setup is that it allows us to distinguish a genuine 4-photon state from two independent pairs by detecting coincidences between two photons in the same arm, as was introduced earlier for 4-photon states in the time-domain [6]. In this setup only the 4-photon states created by stimulated emission generate strong correlations between detectors $D1$ and $D2$, while double pair states do not create any special correlations.

The length of the 2 ps laser pulse is a compromise between a short laser pulse to select a single temporal mode on the one hand and a somewhat longer laser pulse to retain efficient SPDC on the other hand. For a very short laser pulse the photons are created at a well-defined time, but the SPDC process becomes inefficient due to the broad spectral content of the laser pulse. In our study, the combination of the pulse duration and the bandpass filter selects $\sim$3 temporal modes, leading to a maximum possible visibility χ=0.5 for a single spatial mode. The choice of the pulse duration and the length of the crystal was motivated by the group velocity walk-off length L_g = 1.5 mm, calculated for transform-limited pulses, being comparable to the crystal length. Under those conditions, the phase-matching in the crystal is only mildly affected by the pulsed laser and all frequency components of the laser pulse contribute to the efficient generation of SPDC light.
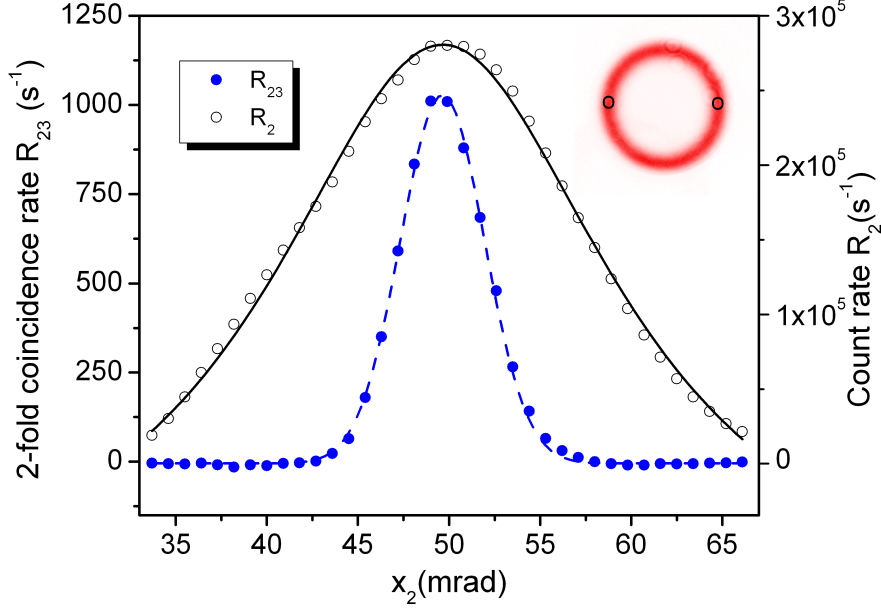
Figure 2.2: *(Color online) Measured single count rates R_2 (open symbols) and 2-fold coincidence rates R_{23} (filled symbols) as a function of position x_2, demonstrating spatial correlations in the two-photon field. The pulsed laser beam was focused in the center of the crystal using a $f = 250$ mm lens. Data are collected using a 1 nm FWHM bandpass filter and a 1.5 mm aperture in the far-field. The solid and dashed lines indicate Lorentzian and Gaussian fits to the single and coincidence rates, respectively. The inset shows a far field image of the SPDC light emitted by the PPKTP crystal at a temperature of 20 °C. The approximate positions of detectors D2 and D3 are shown by circles on the ring.*

2.2.2 Quantum correlations at the two-photon level and number of Schmidt modes

Figure 2.2 shows the measured coincidence rate between detectors $D2$ and $D3$ (solid symbols, left axis) as a function of the position x_2 of detector D_2. Detector assembly D_3 is positioned at a fixed position and collects photons at an angle of -50 mrad in the far-field of the source. The measured coincidences, corrected for accidental events, are compared to the measured single count rate on detector $D2$ (open symbols, right axis). The measured single count rate on detector D_3 is $\sim 3 \cdot 10^5 \ s^{-1}$ and is constant throughout the experiment.

The single count rate as a function of detector position is well described

by a Lorentzian fit (solid line) centered at a position of 50±5 mrad and a width of 14.9±0.5 mrad FWHM. Please note that the uncertainty in the stated center position is due to the fact that it is difficult to determine the absolute position of lens $L2$ on the optical table. The characteristic minima of the sinc^2 phase-matching curve commonly observed under continuous wave pumping are 'averaged' out by the multiple frequencies available in the spectrum of the picosecond pulsed laser [20]. The measured two-fold coincidence rate as a function of the position x_2 of the detector is well described by a Gaussian (dashed line) with a width (FWHM) of 5.1±0.1 mrad, and a center position of 50±5 mrad. The observation that the peak in coincidence rate is much narrower than the measured singles is a clear signature of two-photon correlations in a high-dimensional Hilbert space. The ratio of the width of the singles versus the coincidences is a direct measure of the Schmidt number K_r of the (radial) spatial entanglement generated in the PPKTP crystal [21]. Based on the measured width of the coincidence and singles peak, we estimate a Schmidt number $K_{exp} \approx 2.9\pm0.1$ for the pulsed laser. This estimate should be converted to a two-dimensional Schmidt number in order to compare this number to values given in literature for continuous wave pumping.

To this end, we introduce a second azimuthal Schmidt number K_ϕ, being the ratio of the circumference of the SPDC ring, i.e. $2\pi\times50$ mrad, over the measured width of the coincidence peak. This results in $K_\phi \approx 60\pm6$ and a corresponding Schmidt number $K = K_r K_\phi \approx 175\pm20$. This number should be compared to calculated values [8] and experimental values obtained for a 5.0 mm crystal pumped by a continuous wave laser [21]. The value of K from ref. [21] for strongly negative phase mismatch (i.e. an open SPDC ring) was scaled to our case by taking into account the differences in pump beam waist and crystal length. Based on this, we expect a two-dimensional Schmidt number of ~125. This value is somewhat lower than the value stated above, which we attribute to the fact that we neglected the effect of the pulsed laser on the width of the SPDC ring. The pulsed laser contains many pump frequencies which gives a slightly broader ring and consequently causes an overestimate of the value of K_r.

2.2.3   Observation of quantum correlations of 4-photon states in the spatial degrees of freedom

To explore the contribution of stimulated emission we measure the coincidence rate R_{21} between detectors $D1$ and $D2$. Coincidences can only be registered if at least four photons are generated by a single photon

pulse, since only one-photon in each pair produced by SPDC can be detected. The measured coincidence rate for photons originating from the same pulse contains both stimulated and spontaneous events. To get a measure of the number of coincidences due to spontaneous emission we introduce a tunable electronic delay between detectors $D1$ and $D2$. This allows a measurement of the coincidences in the same laser pulse ($R_{21}^{0\text{ns}}$) as well as the coincidence events between subsequent laser pulses by setting the electronic delay to 12 ns ($R_{21}^{12\text{ns}}$). This latter coincidence rate is dominated by events where a single pair is produced in each of the laser pulses and the coincidence rate $R_{21}^{12\text{ns}}$ thus represents only the coincidence rate due to two spontaneously emitted photon pairs.

The difference in these coincidence rates, normalized by the coincidence rate due to spontaneous events is equal to the "visibility" χ, i.e. $\chi = (R_{21}^{0\text{ns}} - R_{21}^{12\text{ns}})/R_{21}^{12\text{ns}}$ and is a good measure of the extra events due to stimulated emission of 4-photon states. The measured visibility as a function of the position of the two detectors, $\chi(x_1, x_2)$, can be interpreted as a joint spatial density of stimulated pair emission. This joint spatial distribution of stimulated pair emission is depicted in Fig 2.3. The false colour image in Fig. 2.3a shows the difference in coincidence rate ($R_{21}^{0\text{ns}} - R_{21}^{12\text{ns}}$) as a function of the position x_1 and x_2 of detectors $D1$ and D_2 using a 5 nm bandpass filter for the SPDC light. The image is centered around the point $x_1 = x_2 = 50$ mrad and clearly shows the expected positive correlation due to stimualted emission of the 4-photon state that leads to extra coincidences whenever the two detectors detect photons in the same optical mode, i.e. when $x_1 = x_2$. The width (FWHM) of the peak along the diagonal ($x_1 - x_2 = 0$ mrad) is 11.5±0.3 mrad, while the width along the anti-diagonal direction ($x_1 + x_2 = 100$ mrad) is 4.5±0.1 mrad.

Figure 2.3b shows the visibility $\chi(x_1, x_2)$ as a function of position x_2 of detector $D2$ for a fixed position of detector $D1$. The three curves correspond to $x_1 = 44.4$ mrad (triangles), 50.0 mrad (circles) and 55.6 mrad (squares). These data are taken with a 1 nm bandpass filter for the SPDC light in order to enhance the visibility at the expense of a much lower count rate. The narrow band frequency filter lowers the number of temporal modes involved, but does not affect the spatial modes. The integration time per point was increased by repeated scanning of the detector in the x_2 direction. Because the phase-mismatch of the PPKTP crystal that governs the SPDC process depends weakly on laser power, the long term stability of the laser becomes important. In order to correct for this effect we also monitor the single counts on the detector $D2$ as a function of position x_2 and exclude scans from our analysis where the SPDC ring appears shifted. The solid lines through the data are Gaussian fits to the data with
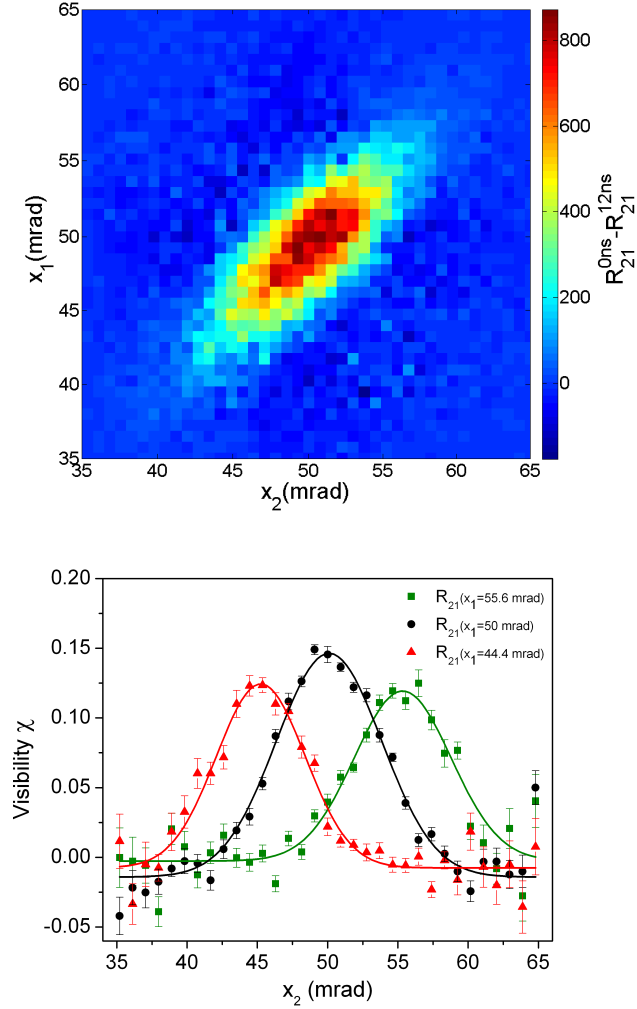
Figure 2.3: *(Color) Measured joint spatial distribution of stimulated pair emission. (a) False-color plot of the measured difference in coincidence rate ($R_{21}^{0ns} - R_{21}^{12ns}$) as a function of the positions of x_1 and x_2 of detectors D_1 and D_2. Data are collected with a 5 nm FWHM bandpass filter and a 1.5 mm aperture size. The observed maximum coincidence rate (R_{21}^{0ns} is typically 25,000 s^{-1}. The data clearly demonstrate that stimulated pair emission occurs when the photons are emitted in the same spatial mode, i.e. when $x_1 = x_2$. (b) Visibility χ of the 4-photon state as a function of position x_2. The different symbols (triangles, circles, squares) correspond to different positions x_1 (44.4, 50.0, 55.6 mrad) of detector D_1. Data are collected using a 1 nm FWHM bandpass filter and a 1.5 mm aperture. The solid lines through the data are Gaussian fits.*

a FWHM width of 8.9±0.3. The peak positions are shifted to the position of detector $D1$, such that the peak of the Gaussian appears at $x_1 = x_2$. The obtained peak visibilities for the three curves are 0.13±0.01, 0.16±0.01 and 0.12±0.01. For a uniform illumination of the aperture one would expect the peak visibility to be independent of the position x_1. This case corresponds to a situation where the width of the SPDC ring, as given by the phase-matching function, is much larger than the shift in position x_1. In our experiment the slightly lower visibility for $x_1 = 44.4$ and 55.6 mrad is caused by the finite diameter of the 1.5 mm aperture that captures a non-uniform part of the SPDC ring. For larger apertures (data not shown) this decrease in visibility indeed becomes more significant.

The visibility in our experiment is limited by both the number of temporal modes collected as well as by the ratio of the total number of spatial modes available over the number of spatial modes collected by the aperture. The total number of temporal modes generated is given by the frequency bandwidth of the SPDC light as compared to the frequency spread of the pulse. For a Fourier limited pulse shape the frequency bandwidth is related to the pulse duration via $\tau = (2\ln(2)\lambda^2)/(\pi c \Delta\lambda)$, where τ is the pulse duration and $\lambda/\Delta\lambda$ is the relative frequency spread. The 2 ps pulse corresponds to an equivalent spectral width of 0.5 nm, while the 2 mm PPKTP crystal produces SPDC light with a bandwidth of ∼40 nm FWHM. Consequently, the number of available temporal modes for a PPKTP crystal pumped by a 2 ps laser is pulse is potentially ∼80. We use '5 nm' and '1 nm' bandpass filters centered at 826.4 nm to limit the number of temporal modes. The measured FWHM bandwidth of these filters is 4.6 nm and 1.5 nm, which extends the coherence time of the SPDC light and limit the number of temporal modes to ∼9 and ∼3 respectively. Since χ is inversely proportional to the number of available temporal modes [6], this produces upper limits to χ of 0.1 and 0.3 for the two bandpass filters. We stress that shorter pump pulses do not necessarily lead to a higher flux of photons since the phase-matching in the 2 mm PPKTP crystal effectively filters the pump pulse. In our experiments we have carefully chosen the crystal length to maximize conversion efficiency without significantly stretching the pump pulse to avoid a non-factorable structure ('X-entanglement') between spatial and temporal degrees of freedom [22].

Figure 2.4 shows the measured visibility as a function of aperture size for a 5 nm bandpass filter (circles) as compared to a 1 nm bandpass filter (triangles). Measurements were performed by measuring coincidence rates between detectors $D1$ and $D2$ at a fixed position $x_1 = x_2 = 50$ mrad. A measurement of the coincidence rate as a function of the electronic time delay is shown in the inset for a point with a relatively high visibility of
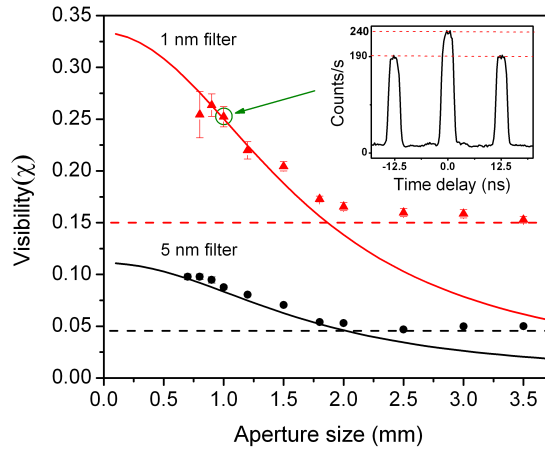
Figure 2.4: *(Color online) Visibility χ of the 4-photon state as a function of aperture size using a 1 nm FWHM bandpass filter (triangles) and a 5 nm FWHM bandpass filter (circles). These data are obtained by subtracting the measured coincidence rate at a delay of 12 ns from the measured coincidence rate at zero delay. Typical single count rates on the detector are 1.4×10^6 and 3×10^5 sec^{-1} for apertures > 2 mm and drop to 5×10^5 and 1×10^5 sec^{-1} for a 1 mm aperture size. The solid lines represent a calculation with no free parameters (see text). For apertures larger than 2 mm, the aperture is limited by lens L3 and the numerical aperture of the fiber and the visibility saturates as indicated by the horizontal dashed lines. The inset shows the measured coincidence rate R_{12} as a function of electronic delay for a 1 nm FWHM bandpass filter and a 1 mm aperture size ($\chi = 0.25$), indicated by the arrow.*

0.25. The extra 50 counts/sec at zero delay are due to stimulated emission of photon pairs. Clearly, the visibility is low and nearly constant for apertures that are larger than 2 mm and rises as the number of available spatial modes is reduced by closing the aperture. In our experiments the visibility saturates at apertures sizes above 2 mm where the apertures size is limited by the finite numerical aperture of the multimode fiber in combination with the focal length of the fiber coupling lens *L*3. The saturation is represented by the horizontal dashed lines.

The visibility χ in the experiment is proportional to the inverse of the number of spatial and temporal modes, i.e. $\chi \propto N_t^{-1} N_{sp}^{-1}$, where N_t and N_{sp} are the number of temporal and spatial modes respectively. Throughout the experiment N_t is determined by the FWHM of the bandpass filter and can be considered constant. We use values of $N_t = 9$ and $N_t = 3$ for the two different bandpass filters. In order to estimate the number of spatial modes collected as a function of aperture size we consider the correlations between two point-like apertures at positions $\mathbf{r_1}$ and $\mathbf{r_2}$. The resulting visibility is given by:

$$\chi(\mathbf{r_1}, \mathbf{r_2}) = \exp\left(-\frac{|\mathbf{r_1} - \mathbf{r_2}|^2}{r_0^2}\right). \tag{2.3}$$

The characteristic distance $r_0 = (\lambda f_2)/(\pi w_p)$, where $f_2 = 270$ mm is the focal distance of lens *L*2 that creates the far-field of the SPDC source and w_p is the waist of the pump beam created by focussing the pump beam using lens *L*1. Using the measured waist of the pump beam of 80 μm we find a characteristic distance $r_0 = 0.9$ mm. The visibility in the experiment due to finite aperture size for two apertures centered at the same position can be found via integration:

$$\chi(a) = \frac{1}{N_t \pi^2 a^4} \iint \chi(\mathbf{r_1}, \mathbf{r_2}) \Theta(|\mathbf{r_1}| - a) \Theta(|\mathbf{r_2}| - a) \mathrm{d}\mathbf{r_1} \mathrm{d}\mathbf{r_2}, \tag{2.4}$$

where the Heaviside step-functions $\Theta(|\mathbf{r_1}| - a)$ and $\Theta(|\mathbf{r_2}| - a)$ represent the sharp edges of the two apertures with equal radius a in the far-field. The solid lines through the data in Fig. 2.4 are the results of calculating the double integral represented by equation 2.4 using 3 and 9 temporal modes for the two bandpass filters and the calculated value of r_0 based on the measured beam waist. The agreement between the data and the model with no adjustable parameters is striking for aperture sizes below 2 mm. For apertures above 2 mm the visibility saturates, as indicated by the horizontal dashed lines, at a value determined by lens *L*3 and the numerical aperture of the multimode fiber that limit the beam diameter to $\sim$2 mm.

2.3 Conclusion

In conclusion, we have demonstrated the existence of spatial correlations between photon pairs in a 4-photon state. These correlations are induced via stimulated pair emission. In our experiments we are able to separate the contribution from spontaneous parametric down-conversion and stimulated parametric down-conversion at the level of double pairs. The stimulated emission becomes important when a 2 mm long PPKTP crystal is pumped by a 2 ps pulsed laser at 413.2 nm wavelength to create frequency and polarization degenerate photon pairs at a wavelength of 826.4 nm. The spatial correlations of the stimulated photon pairs contains a rich structure when using a non-colinear geometry for the down-conversion process, which can be explored with relative ease using apertures in the far-field. In this way we present the first measurements of the joint spatial distribution of stimulated pair emission and discuss the acquired visibility. This technique opens new possibilities to explore the structure of higher-dimensional entanglement by making use of spatial degrees of freedom instead of the temporal degree of freedom. The possibility to distinguish between stimulated and spontaneous processes can be used to explore recent proposals for ghost imaging with thermal and quantum light sources[23, 24].

Acknowledgements

Bibliography

[1] S. L. Braunstein and P. van Loock, *Quantum information with continuous variables*, Rev. Mod. Phys. **77**, 513 (2005).

[2] Z. Y. Ou and L. Mandel, *Observation of spatial quantum beating with separated photodetectors*, Physical Review Letters **61**, 54 (1988).

[3] X. Li, L. Yang, X. Ma, L. Cui, Z. Y. Ou, and D. Yu, *All-fiber source of frequency-entangled photon pairs*, Physical Review A **79**, 033817 (2009).

[4] S. Friberg, C. K. Hong, and L. Mandel, *Measurement of Time Delays in the Parametric Production of Photon Pairs*, Physical Review Letters **54**, 2011 (1985).

[5] Z. Y. Ou, J. K. Rhee, and L. J. Wang, *Observation of Four-Photon Interference with a Beam Splitter by Pulsed Parametric Down-Conversion*, Physical Review Letters **83**, 959 (1999).

[6] H. D. Riedmatten, V. Scarani, I. Marcikic, A. Acín, W. Tittel, H. Zbinden, and N. Gisin, *Two independent photon pairs versus four-photon entangled states in parametric down conversion*, Journal of Modern Optics **51**, 1637 (2004).

[7] D. Strekalov, A. Sergienko, and D. Klyshko, *Observation of Two-Photon "Ghost" Interference and Diffraction*, Physical review letters **74**, 3600 (1995).

[8] C. K. Law and J. H. Eberly, *Analysis and Interpretation of High Transverse Entanglement in Optical Parametric Down Conversion*, Physical Review Letters **92**, 127903 (2004).

[9] J. C. Howell, R. S. Bennink, S. J. Bentley, and R. W. Boyd, *Realization of the Einstein-Podolsky-Rosen Paradox Using Momentum- and Position-Entangled Photons from Spontaneous Parametric Down Conversion*, Physical Review Letters **92**, 210403 (2004).

[10] S. Walborn, C. Monken, S. Pádua, and P. Souto Ribeiro, *Spatial correlations in parametric down-conversion*, Physics Reports **495**, 87 (2010).

[11] P.-L. de Assis, M. A. D. Carvalho, L. P. Berruezo, J. Ferraz, I. F. Santos, F. Sciarrino, and S. Pádua, *Control of quantum transverse correlations on a four-photon system*, Optics Express **19**, 2868 (2011).

[12] D. Greenberger, M. Horne, and A. Zeilinger, *Bell's Theorem, Quantum Theory, and Conceptions of the Universe*, pages 73–76, Kluwer Academics, Dordrecht, The Netherlands, 1989.

[13] W. Dür, G. Vidal, and J. I. Cirac, *Three qubits can be entangled in two inequivalent ways*, Physical Review A **62**, 062314 (2000).

[14] I. Marcikic, H. de Riedmatten, W. Tittel, V. Scarani, H. Zbinden, and N. Gisin, *Time-bin entangled qubits for quantum communication created by femtosecond pulses*, Physical Review A **66**, 062308 (2002).

[15] R. H. Hadfield, *Single-photon detectors for optical quantum information applications*, Nature Photonics **3**, 696 (2009).

[16] M. D. Eisaman, J. Fan, a. Migdall, and S. V. Polyakov, *Invited Review Article: Single-photon sources and detectors*, Review of Scientific Instruments **82**, 071101 (2011).

[17] C. Simon, G. Weihs, and A. Zeilinger, *Optimal quantum cloning via stimulated emission*, Physical review letters **84**, 2993 (2000).

[18] P. Kok and S. L. Braunstein, *Postselected versus nonpostselected quantum teleportation using parametric down-conversion*, Physical Review A **61**, 042304 (2000).

[19] W. H. Peeters and M. P. van Exter, *Optical characterization of periodically-poled KTiOPO4.*, Optics express **16**, 7344 (2008).

[20] T. E. Keller and M. H. Rubin, *Theory of two-photon entanglement for spontaneous parametric down-conversion driven by a narrow pump pulse*, Physical Review A **56**, 1534 (1997).

[21] H. Di Lorenzo Pires, C. Monken, and M. P. van Exter, *Direct measurement of transverse-mode entanglement in two-photon states*, Physical Review A **80**, 022307 (2009).

[22] A. Gatti, E. Brambilla, L. Caspani, O. Jedrkiewicz, and L. A. Lugiato, *X Entanglement: The Nonfactorable Spatiotemporal Structure of Biphoton Correlation*, Phys. Rev. Lett. **102**, 223601 (2009).

[23] K. W. C. Chan, M. N. O'Sullivan, and R. W. Boyd, *Two-color ghost imaging*, Phys. Rev. A **79**, 033808 (2009).

[24] M. N. O'Sullivan, K. W. C. Chan, and R. W. Boyd, *Comparison of the signal-to-noise characteristics of quantum versus thermal ghost imaging*, Phys. Rev. A **82**, 053803 (2010).